mathematics

MDPI

Article

Complexity-Efficient Coherent Physical Cell Identity Detection Method for Cellular IoT Systems

Young-Hwan You [1,*], Yong-An Jung [2], Sung-Hun Lee [2] and Intae Hwang [3,4]

[1] Department of Computer Engineering and Convergence Engineering for Intelligent Drone, Sejong University, Seoul 05006, Korea
[2] ICT Convergence Research Division, Intelligent Device Research Center, Gumi Electronics & Information Technology Research Institute (GERI), Gumi 39171, Korea
[3] Department of Electronic Engineering, Chonnam National University, Yongbong-ro, Buk-gu, Gwangju 61186, Korea
[4] Department of ICT Convergence System Engineering, Chonnam National University, Yongbong-ro, Buk-gu, Gwangju 61186, Korea
* Correspondence: yhyou@sejong.ac.kr

Abstract: Narrowband Internet of Things (NB-IoT) is one of the low-power wide-area network technologies that aim to support enormous connection, deep coverage, low power consumption, and low cost. Therefore, low cost of implementation and maintenance is one of the key challenges of NB-IoT terminals. This paper presents a low-complexity formulation for narrowband secondary synchronization signal (NSSS) detection in the NB-IoT system, supported by a coherent algorithm that requires a priori knowledge of the channel. By exploiting a symmetric conjugate feature of the NSSS sequence, a joint physical cell ID and radio frame number detection method with low complexity is proposed for coherent detection. The probability of erroneous detection of the presented NSSS detection method is computed, and the analytical model is verified by means of simulation. Numerical experiments will demonstrate that the proposed detection scheme remarkably reduces the computational complexity with almost the same detection ability compared to the existing detection scheme.

Keywords: Narrowband Internet of Things; secondary synchronization signal; physical cell ID; radio frame number

MSC: 94A13

Citation: You, Y.-H.; Jung, Y.-A.; Lee, S.-H.; Hwang, I. Complexity-Efficient Coherent Physical Cell Identity Detection Method for Cellular IoT Systems. *Mathematics* **2022**, *10*, 3024. https://doi.org/10.3390/math10163024

Academic Editors: Yang Liu and Jakub Nalepa

Received: 19 July 2022
Accepted: 19 August 2022
Published: 22 August 2022

1. Introduction

Recently, ultra-low-end Internet of Things (IoT) applications have been gaining great attention in areas such as smart home automation, industrial process automation, remote manufacturing, unmanned aerial system, and intelligent transportation systems [1–4]. To satisfy the requirements of IoT, many low-power wide-area (LPWA) techniques working in licensed frequency bands were developed [5–7]. Among various LPWA standards, narrowband IoT (NB-IoT) is the most popular technique due to its ability to have massive connections as it is inherited from long-term evolution (LTE). Thus, one of the key challenging concerns of NB-IoT is the low cost of implementation, deployment, and maintenance because they can be cheap, widely dispersed, and even disposable [8,9]. Moreover, similar to LTE, every device must be synchronized with an enhanced base station (eNodeB) to connect the network. Typically, user equipment (UE) needs to continuously obtain timing information and search for physical cell ID (PCID) at power-up [10–12]. The process of performing network synchronization and identifying any available eNodeB by a NB-IoT UE is termed as the initial cell search. To assist such a task, the UE needs to detect two specific signals broadcasted from the eNodeB: narrowband primary synchronization signal (NPSS) and narrowband secondary synchronization signal (NSSS).

In order to reliably maintain a connection between UE and serving eNodeB, the NB-IoT device has to perform a series of tasks of finding the symbol timing offset (STO) and estimating the carrier frequency offset (CFO) in a pre-discrete Fourier transform (DFT) stage. To perform these tasks, autocorrelation and cross-correlation have been proved to be an efficient solution [11–13]. Once time and frequency uncertainties have been resolved by exploiting the NPSS, a cyclic prefix (CP) can be removed, and the NB-IoT UE performs a DFT to convert the CP-removed signal to the frequency domain. In a post-DFT step, the NB-IoT device attempts to detect the PCID and radio frame number (RFN) by observing multiple NSSS preambles. If the NB-IoT device fails to identify the NSSS, it has to fully scan the available frequency band, significantly increasing power consumption [11].

Most NB-IoT UEs are usually implemented with less expensive crystal oscillators resulting in CFO of as much as 20 ppm [12]. Therefore, there exist non-negligible time and frequency offsets between the NB-IoT UE and the network, and such uncertainties may cause difficulty in establishing an initial connection. Despite the large uncertainties, an NB-IoT UE needs to be able to a perform reliable cell search at a very low signal-to-noise ratio (SNR). Recently, a significant number of detection methods have been developed to identify the NSSS [12–20]. An exhaustive maximum likelihood (ML) method proposed in [12] attains optimal detection performance at the expense of the computational burden. By exploiting the property that the complementary Walsh sequences composing the NSSS are binary-modulated, several simplifications have been suggested in [13–15]. However, the simplified methods no longer take advantage of NSSS properties in spite of decreasing the computational burden. By using inherent features of an NSSS sequence, the authors of [16–18] proposed suboptimal alternatives to significantly reduce the complexity without relying on a priori knowledge of the channel. Since such non-coherent methods are originally developed assuming flat-fading conditions, the detection performance is severely degraded in the presence of the frequency selectivity. A differential correlation strategy can be used to remove the effects of the channel fading [19]. However, the differential detection approach developed in the LTE system is not directly applied to the NB-IoT system due to the loss of the autocorrelation property of the NSSS. In [20], a DFT-based coherent NSSS detector has been developed, which is based on algorithms for fast computations of DFTs to perform the cross-correlation, thereby reducing the complexity of the NSSS detector. However, when considering other computational complexities together to estimate the channel, the DFT-based detection method is too computationally expensive since NB-IoT needs to compare 4032 potential NSSS candidates. Therefore, the NB-IoT device has to provide a complexity-effective and robust NSSS detection method that guarantees battery lifetimes greater than 10 years for low data-rate IoT applications.

This paper proposes an effective coherent joint PCID and RFN detection scheme in the cellular NB-IoT system. The basic idea is to decouple the joint search space of the NSSS detection into a small number of hypotheses, which contributes to reducing the processing burden. To do so, the symmetric conjugate property of the NSSS sequence is explored. To validate the effectiveness of the proposed NSSS detection method, the probability of erroneous detection (PED) is analytically computed. The numerical analysis is verified by simulation results and proven to be very accurate. Simulations demonstrate that the proposed coherent detection method obtains the PCID and RFN with reduced computational complexity while achieving almost a similar performance to the existing coherent detection method. If an average estimation is adopted to improve detection performance of NB-IoT UEs in a poor coverage area, the proposed coherent detector requires only half the complexity of the conventional coherent detector to maintain a target error rate at the cost of a slight increase in the processing delay.

The remaining part of this paper is structured as follows. The related work in NSSS detection is reviewed in Section 2. Section 3 presents the signal model and synchronization signal in the cellular NB-IoT system. In Section 4, we propose an improved coherent NSSS detection method and the PED of the proposed detection method is numerically derived.

Section 5 presents the comprehensive simulation result to assess the usefulness of the proposed NSSS detection method. The paper is concluded in Section 6.

Notations: The operators $\mathbb{E}\{\cdot\}$ and $\lfloor\cdot\rfloor$ are used to represent the expected value and rounding-down operation of the enclosed variable, respectively. The superscripts X^*, X^I, and X^Q represent the complex conjugation, real part, and imaginary part of a complex variable X, respectively. The magnitude and argument of a complex number X are denoted by $|X|$ and $\angle\{X\}$, respectively, leading to $X = |X|e^{j\angle\{X\}}$. The notation $G \sim \mathcal{G}(\mu, \sigma^2)$ means that G is the real-valued normal distribution with mean μ and variance σ^2. Finally, $\cosh(x)$ is the hyperbolic cosine function, $Q(x)$ is the Q-function, $I_0(x)$ is the zeroth-order modified Bessel function of the first kind, and $\mathrm{mod}(x, y)$ is the modulus operation that returns the integer remainder of x/y. Table 1 summarizes the variables used in the paper.

Table 1. Main variables used in this paper.

Notation	Description
x^*	Complex conjugation of a complex number x
$\|x\|$	Magnitude of a complex number x
$\angle\{x\}$	Argument of a complex number x
x^I	Real part of a complex variable x
x^Q	Imaginary part of a complex variable x
$\lfloor x \rfloor$	Rounding-down operation of variable x
$\mathbb{E}\{x\}$	Expected value of variable x
$\hat{x}$	Estimate of variable x
$\mathrm{mod}(x, y)$	Modulus operation which returns the integer remainder of x/y
(ϵ, ε)	(CFO, residual CFO)
(θ, ϑ)	(STO, residual STO)
(v, n_r)	(PCID, RFN)
m	Index for deciding the RFN in which the NSSS is transmitted
n	Cell specific parameter given by $n = \lfloor v/126 \rfloor$
u	Cyclic shift given by $u = \mathrm{mod}(n_r/8, 4)$
w	Root sequence given by $w = \mathrm{mod}(v, 126) + 3$
(a, b, c, d)	Hypothesized number for (m, n, u, w)
$B_{l,k}(n)$	Hadamard–Walsh sequence derived from $c_n(g')$
$C_{l,k}(u)$	Sequence derived from $e^{-j2\pi ug}$
$D_{l,k}(w)$	Zadoff–Chu sequence derived from $e^{-j\pi wg''(g''+1)/131}$
$E_{l,k}(n, u, w)$	NSSS sequence derived from $B_{l,k}(n)$, $C_{l,k}(u)$, and $D_{l,k}(w)$
$\mathcal{S}$	Set of NSSS subcarrier index

2. Related Works

The NSSS detection method can be categorized into two major groups: non-coherent approach and coherent approach. The former has been considered as an effective approach to detect the NSSS without resorting to the channel information in flat-fading condition [12–18]. Full-search-based ML strategy developed in [12] gives an optimal solution at the cost of implementation burden because all the possible realizations of Zadoff–Chu (ZC) and Hadamard–Walsh sequences have to be compared to the received NSSS observation. In particular, the NB-IoT receiver needs to hypothesize 4032 possible candidates of the NSSS sequence to simultaneously detect both PCID and RFN, which enforces high computational complexity in the initial cell search procedure. To tackle this challenge, reduced-complexity solutions have been proposed exploiting the feature that some components of NSSS sequences can be implemented without multiplication operation [13–15]. By using inherent properties of the NSSS sequence, these methods give suboptimal solutions with a remarkable reduction in computational burden when compared to an optimal full-search-based ML method. Based on the property that complementary Walsh sequences are binary-modulated and ZC sequences are repeated in the frequency domain, the works in [13,14] significantly save the computational burden in the NSSS detection. To decouple the joint detection task of the PCID and RFN, a sequential detection method without fully performing hypothesis testing on NSSS candidates was proposed in [15]. Despite reducing

their complexity, such cross-correlation-based approaches no longer take advantage of NSSS properties to perform the NSSS detection, inevitably leading to considerable performance degradation. In spite of the investigation in [13–15], such suboptimal detectors would still become impractical since their structural complexity is proportional to the number of hypothesis testing. Authors in [16–18] developed near-ML but low complexity NSSS detection methods. In [16], a near-ML method was presented using autocorrelation of the NSSS instead of cross-correlation. This approach is based on the symmetric property of the ZC sequence, which leads to a reduced-complexity NSSS detector. In [17], the NSSS detection is performed by detecting the ZC and Hadamard–Walsh sequences in two steps, which contributes to decreasing the arithmetic operation. However, such an advantage is obtained at the price of a slight degradation in detection accuracy. Another simplification was proposed in [18], which is based on an NSSS subcarrier grouping algorithm to detect the NSSS with reduced computational burden. Compared to ML detection, this alternative solution greatly reduces the computational complexity without sacrificing detection capability at the expense of slightly increased processing latency. Since such non-coherent methods in [16–18] are originally developed to achieve near-ML performance in a flat-fading condition, they do not overcome the effect of the frequency-selective fading of the channel despite reducing the computational complexity. To cope with the effect of the channel fading distortion, a differential correlation-based non-coherent approach and channel-estimation-based coherent approach can be used [19,20]. The authors of [19] proposed a differential correlation-based joint detection of synchronization signals in the LTE system, and suboptimal performance is achieved with reduced complexity in a decoupled manner. Unfortunately, this detection method is not directly applicable to the NB-IoT system due to poor autocorrelation characteristics of the NSSS sequence. In [20], a DFT-based NSSS detection approach was proposed for both situations where the channel is unknown and has to be estimated. In the case of the flat-fading channel, this method can be designed using DFT operations with a comparable complexity to the approach in [14]. On the other hand, applying this coherent detection approach to combat frequency-selective fading requires a significant increase in the complexity of channel estimation, as this task has to be performed for 4032 possible hypotheses. Accordingly, NSSS detection plays a key role in the initial synchronization procedure of NB-IoT because the NSSS is associated with both PCID and RFN.

3. System Description

3.1. Signal Model

For an orthogonal frequency division multiplexing (OFDM) system using N equispaced subcarriers, a complex data symbol inserted on the k-th subcarrier of the l-th symbol is represented by $X_{l,k}$. An OFDM symbol is generated by performing N-point inverse DFT (IDFT) to produce N complex time-domain samples. To maintain inter-symbol orthogonality and remove inter-carrier interference (ICI), a CP is appended to each symbol before transmitting duration T_g sec such that an effective OFDM symbol of duration $T_u = (N + N_g)T_s = (1 + N_g/N)/\Delta_f$ is created, where T_s denotes the sampling time period at the transmitter, N_g is the length of CP, and Δ_f is the minimum subcarrier spacing. Therefore, the time-domain sample of the OFDM symbol during the l-th symbol period is given as

$$x_{l,q} = \sum_{k=0}^{N-1} X_{l,k} e^{j2\pi kq/N},\ q = -N_g, -N_g + 1, \cdots, N - 1 \tag{1}$$

The transmitted signal is subject to multipath fading and additive noise pollution introduced by the channel. After passing through a multipath fading channel, the radio frequency signal with central carrier frequency f_c is down-converted to an OFDM baseband

with an oscillator frequency $f_c^{'}$. Then, the time-domain sampled signal at a rate of $1/T_s$ can be obtained as

$$y_{l,q} = e^{j2\pi l\epsilon\rho_1} e^{j2\pi\epsilon(q-\theta)/N} \sum_{p=1}^{L} h_{l,p} x_{l,q-\tau_p-\theta} + z_{l,q} \tag{2}$$

where $\rho_1 = (N+N_g)/N = N_t/N$, $q = -N_g, -N_g+1, \cdots, N-1$, $h_{l,p}$ denotes the discrete-time impulse response of the channel with L resolvable multipaths, τ_p denotes the relative delay of the p-th path, $z_{l,q}$ denotes the zero-mean additive white Gaussian noise (AWGN) with variance σ_z^2, $\epsilon = (f_c - f_c^{'})/\Delta_f$ is the normalized CFO, and θ denotes the initial STO. Since any fractional STO is incorporated into $h_{l,p}$, θ can be treated to be integer-valued.

Based on the received signal $y_{l,q}$, the NB-IoT device tries to find a coarse STO estimate $\hat{\theta}$ and CFO estimate $\hat{\epsilon}$, which have to be removed from $y_{l,q}$ in the time domain [13,14]. Even after these initial ambiguities have been removed, residual CFO $\varepsilon = \epsilon - \hat{\epsilon}$ and residual STO $\vartheta = \theta - \hat{\theta}$ possibly remain. Based on the estimates in the pre-DFT step, the CP is extracted from the received signal, and a DFT process is performed. Afterward, the DFT output at the k-th subcarrier of the l-th symbol can be written as [21,22]

$$Y_{l,k} \approx H_{l,k} X_{l,k} e^{-j2\pi k\vartheta/N} e^{j2\pi\varepsilon(l\rho_1+\rho_2)} + I_{l,k} + Z_{l,k} \tag{3}$$

where $\rho_2 = N_g/N$, $H_l(k)$ denotes the channel frequency response with variance σ_H^2, $I_{l,k}$ denotes the ICI component with variance $\sigma_I^2 \approx \mathbb{E}\{|X_{l,k}|^2\}\sigma_H^2\varepsilon^2\pi^2/3$, and $Z_{l,k}$ denotes an identically distributed circularly symmetric complex Gaussian random process with variance σ_Z^2. For practical values of ε, σ_I^2 is negligible compared to the noise power, and thus, the ICI component can be neglected during the post-DFT step [21].

3.2. Synchronization Signal

In the NB-IoT downlink, each frame is 10 ms in length in the time domain and consists of 10 subframes. A subframe is divided into 2 slots each, including 7 OFDM symbols. There are two kinds of dedicated signals such as narrowband reference signals (NRS) and synchronization signals in NB-IoT. The NRS is dedicated to channel estimation, whereas the synchronization signals that include the NPSS and the NSSS are mainly used to perform an initial cell search. For this purpose, the NPSS is periodically transmitted in subframe 5 in every 10 ms frame, whereas the NSSS is transmitted in subframe 9 in frames with 20 ms periodicity. After the power is turned on, the NB-IoT UE performs the time and frequency estimation procedure by synchronizing to NPSS. Since the NPSS is common in every subframe for all eNodeBs, the NB-IoT UE needs to search for only one NPSS sequence. On the other hand, the NSSS is dedicated to performing full downlink synchronization by detecting the PCID and acquiring the timing information within an 80 ms block.

Both NPSS and NSSS sequences are generated from the frequency-domain ZC sequences [23]. The NPSS is formulated to be robust to the presence of a large CFO and is derived from length-11 ZC sequence of root index 5, thus taking the form

$$P_{l,k} = A_l e^{-j5\pi k(k+1)/11},\ 0 \le k < 11, 3 \le l < 14 \tag{4}$$

where $A_l = \{1,1,1,1,-1,-1,1,1,1,-1,1\}$ is the binary cover code. In every fifth subframe, $P_{l,k}$ is located in the last 11 consecutive OFDM symbols, each of which consists of 12 subcarriers. Each of 11 OFDM symbols in an NPSS subframe carries a copy of the base sequence based on $A_l \in \{-1,1\}$. Therefore, NB-IoT supports 504 unique PCIDs indicated by NSSS, which can be transmitted in every even-numbered frame. The NSSS is derived by element-wise multiplication between a ZC sequence and a Hadamard–Walsh

sequence. Specifically, the NSSS is scrambled with a frame-dependent sequence code and takes the form

$$E_g = c_{n,g'} e^{-j2\pi ug} e^{-j\pi wg''(g''+1)/(N_s-1)},\ 0 \le g < N_s \tag{5}$$

where $N_s = 132$ denotes the length of the NSSS sequence, $n = \lfloor v/126 \rfloor$, $v \in \{0, 1, 2, \cdots, 503\}$ denotes the PCID, $g' = \mathrm{mod}(g, 128)$, $g'' = \mathrm{mod}(g, 131)$, $w = \mathrm{mod}(v, 126) + 3$, $u = \mathrm{mod}(n_r/8, 4)$ is decided by the RFN n_r, and $c_{n,g'}$ is based on length-128 Hadamard–Walsh sequences with the first four components cyclically suffixed to form a length-132 sequence [7].

To simplify the notation, E_g is grouped into 11 equally-sized successive blocks, which are sequentially allocated to 11 OFDM symbols. Accordingly, the transmission bandwidth of the NPSS and NSSS is only one resource block (RB) consisting of 12 subcarriers. Based on this notation, the l-th symbol at the k-th subcarrier is symbolized as $E_{l,k}(n, u, w)$ for $3 \le l \le 13$ and $0 \le k < 12$. Mapping from E_g to $E_{l,k}(n, u, w)$ is performed in increasing order of first the index k and then the index l. Let $B_{l,k}(n)$, $C_{l,k}(u)$ and $D_{l,k}(w)$ be sequences generated from $c_n(g')$, $e^{-j2\pi ug}$ and $e^{-j\pi wg''(g''+1)/131}$, respectively. For the purpose of brevity, let the NSSS be composed of three concatenated sequences so that

$$E_{l,k}(n, u, w) = B_{l,k}(n) C_{l,k}(u) D_{l,k}(w) \tag{6}$$

where $n \in \{0, 1, 2, 3\}$, $u \in \{0, 1/4, 2/4, 3/4\}$, and $w \in \{3, 4, \cdots, 128\}$.

4. Proposed Joint Detection Scheme

In this section, a complexity-efficient NSSS detector in the NB-IoT communication system is presented. For this aim, the joint detection task of the PCID and RFN is decoupled in a sequential manner. Based on the sequential detection strategy, a low-complexity NSSS detector is designed, and the detection performance of the proposed scheme is evaluated in terms of the PED.

4.1. Detection Algorithm

To focus on the NSSS detection, suppose the channel is constant during one subframe, which is suitable for the situation where the NB-IoT device moves at low speed. Within one subframe, the estimated channel at the k-th subcarrier can be given as

$$\hat{H}_k(a, b, c, d) = \frac{1}{11E_X} \sum_{l=aN_f+3}^{aN_f+13} Y_{l,k} E^*_{l,k}(b, c, d),\ k \in \mathcal{S} \tag{7}$$

where $E_X = |E_{l,k}(b, c, d)|^2$, $\mathcal{S} = \{k | 0 \le k < 12\}$ denotes the full set of the NSSS subcarrier index, $a \in \{0, 1\}$ denotes the hypothesized number for deciding the RFN in which the NSSS is transmitted, $b \in \{0, 1, 2, 3\}$ denotes the hypothesized number for n, $c \in \{0, 1/4, 2/4, 3/4\}$ is the hypothesized number for u, $d \in \{3, 4, \cdots, 128\}$ denotes the hypothesized number for w, and N_f denotes the number of OFDM blocks in a radio frame. The average estimate over one subframe can improve estimation accuracy by mitigating the effect of noise on the estimated channel.

Once the channel fading has been compensated using (7), we obtain the objective function given by

$$\Omega(a, b, c, d) = \sum_{k \in \mathcal{S}} \sum_{l=aN_f+3}^{aN_f+13} \tilde{Y}_{l,k}(a, b, c, d) E^*_{l,k}(b, c, d) \tag{8}$$

where $\tilde{Y}_{l,k}(a, b, c, d) = Y_{l,k} \hat{H}^*_k(a, b, c, d)$. Due to the use of the estimated channel, the proposed NSSS detection method falls into the category of a coherent approach. For conve-

nience, we hereafter omit the notation (a,b,c,d) in $\tilde{Y}_{l,k}(a,b,c,d)$ and $\hat{H}_k(a,b,c,d)$, assuming perfect channel knowledge. When hypothesized numbers exactly match corresponding actual numbers, i.e., $(a,b,c,d)=(m,n,u,w)$, substituting (3) into (8) gives

$$\begin{aligned}\Omega(a,b,c,d) = &\sum_{k\in\mathcal{S}} H_{l,k}\hat{H}_k^* E_X \sum_{l=aN_f+3}^{aN_f+13} e^{j2\pi(\varepsilon(l\rho_1+\rho_2)-k\vartheta/N)} \\ &+ \sum_{k\in\mathcal{S}}\sum_{l=aN_f+3}^{aN_f+13} Z_{l,k}\hat{H}_k^*(a,b,c,d)E_{l,k}^*(b,c,d)\end{aligned} \tag{9}$$

In this case, when $(a,b,c,d)=(m,n,u,w)$, (7) takes the form

$$\hat{H}_k = \frac{H_{l,k}}{11}\sum_{l=aN_f+3}^{aN_f+13} e^{j2\pi(\varepsilon(l\rho_1+\rho_2)-k\vartheta/N)} + \frac{1}{11E_X}\sum_{l=aN_f+3}^{aN_f+13} Z_{l,k}E_{l,k}^*(b,c,d) \tag{10}$$

which is further derived as

$$\hat{H}_k = \frac{H_{l,k}S(\varepsilon)}{11} e^{j2\pi(\varepsilon(5\rho_1+(aN_f+3)\rho_1+\rho_2)-k\vartheta/N)} + \frac{1}{11E_X}\sum_{l=aN_f+3}^{aN_f+13} Z_{l,k}E_{l,k}^*(b,c,d) \tag{11}$$

where $S(\varepsilon)=\sin(22\pi\varepsilon\rho_1)/\sin(2\pi\varepsilon\rho_1)\approx 11$ for sufficiently small values of ε. It is worthy of mentioning that the phase rotation due to ε and ϑ is incorporated into the estimated channel (11), and can thus be compensated from (9).

Since the choice of d and $131-d$ produces ZC sequences, which are complex-conjugates of each other so that $D_{l,k}^*(d)=D_{l,k}(131-d)$, the real part of (8) is in the form

$$\Omega^I(a,b,c,d) = \sum_{k\in\mathcal{S}}\sum_{l=aN_f+3}^{aN_f+13} \tilde{Y}_{l,k}^I E_{l,k}^I(b,c,d') + (-1)^\lambda \sum_{k\in\mathcal{S}}\sum_{l=aN_f+3}^{aN_f+13} \tilde{Y}_{l,k}^Q E_{l,k}^Q(b,c,d') \tag{12}$$

where λ is defined as

$$\lambda = \begin{cases} 0, & \text{for } 3\le d\le 65 \\ 1, & \text{for } 66\le d\le 128 \end{cases} \tag{13}$$

and $d'=d-\lambda(2d-131)\in\{3,4,\cdots,65\}$. It should be noted from (12) that the uncertainty related with two ZC root indices d and $131-d$ is only the sign in the second component of the right-hand side (RHS). Thus, the objective functions for d and $131-d$ can be derived from combinations of identical observation. Using this property, the objective function with reduced search space is formulated as

$$\Psi^I(a,b,c,d') = \sum_{k\in\mathcal{S}}\sum_{l=aN_f+3}^{aN_f+13} \tilde{Y}_{l,k}^I E_{l,k}^I(b,c,d') + \left|\sum_{k\in\mathcal{S}}\sum_{l=aN_f+3}^{aN_f+13} \tilde{Y}_{l,k}^Q E_{l,k}^Q(b,c,d')\right| \tag{14}$$

where $d'\in\{3,4,\cdots,65\}$ denotes the hypothesized number for w' and the quantity $(-1)^\lambda$ that is a function of ZC root index d is eliminated by taking the absolute value of the second term of the RHS in (12).

We focus on the case where $\hat{H}_k=H_{l,k}$ in all subsequent derivations. However, the effect of channel estimation error on the system performance will be evaluated in the simulations. By substituting $\tilde{Y}_{l,k}$ to (14), $\Psi^I(a,b,c,d')$ takes the expression

$$\Psi^I(a,b,c,d') = \sum_{k\in\mathcal{S}} \sum_{l=aN_f+3}^{aN_f+13} |H_{l,k}|^2 X^I_{l,k} E^I_{l,k}(b,c,d') + \mathcal{Z}^I + \left| \sum_{k\in\mathcal{S}} \sum_{l=aN_f+3}^{aN_f+13} |H_{l,k}|^2 X^Q_{l,k} E^Q_{l,k}(b,c,d') + \mathcal{Z}^Q \right| \tag{15}$$

with

$$\mathcal{Z}^{I/Q} = \sum_{k\in\mathcal{S}} \sum_{l=aN_f+3}^{aN_f+13} \tilde{Z}^{I/Q}_{l,k} E^{I/Q}_{l,k}(b,c,d') \tag{16}$$

where $\tilde{Z}_{l,k} = Z_{l,k}\hat{H}^*_k$ and I/Q notation stands for the corresponding term-wise pair. Under hypothesis H_1 that the NSSS signal is correctly detected, i.e., $(a,b,c,d') = (m,n,u,w')$, it follows that $X^{I/Q}_{l,k} E^{I/Q}_{l,k}(b,c,d') = |E^{I/Q}_{l,k}(b,c,d')|^2$. Based on this observation, $\Psi^I(a,b,c,d')$ is given by

$$\Psi^I(a,b,c,d') = \sum_{k\in\mathcal{S}} \sum_{l=aN_f+3}^{aN_f+13} |H_{l,k}|^2 E_X/2 + \mathcal{Z}^I + \left| \sum_{k\in\mathcal{S}} \sum_{l=aN_f+3}^{aN_f+13} |H_{l,k}|^2 E_X/2 + \mathcal{Z}^Q \right| \tag{17}$$

Under hypothesis H_0 that $(a,b,c,d') \neq (m,n,u,w')$, it follows that $X^{I/Q}_{l,k} E^{I/Q}_{l,k}(b,c,d')$ are random sequences since $X_{l,k}$ is treated as a random complex number in a downlink shared channel or a downlink control channel. Therefore, a central limit theorem invokes that $\sum_{k\in\mathcal{S}} \sum_{l=aN_f+3}^{aN_f+13} |H_{l,k}|^2 X^I_{l,k} E^I_{l,k}(b,c,d') + \mathcal{Z}^I$ in (15) is zero-mean Gaussian distributed. Similarly, this distribution also applies to the quantity $\sum_{k\in\mathcal{S}} \sum_{l=aN_f+3}^{aN_f+13} |H_{l,k}|^2 X^Q_{l,k} E^Q_{l,k}(b,c,d') + \mathcal{Z}^Q$. Hence, $|\sum_{k\in\mathcal{S}} \sum_{l=aN_f+3}^{aN_f+13} |H_{l,k}|^2 X^Q_{l,k} E^Q_{l,k}(b,c,d') + \mathcal{Z}^Q|$ is treated as a folded normal random variable under hypothesis H_0.

The proposed NSSS detector comprises two steps. Specifically, a joint detection of the PCID and RFN can be decoupled into two sequential detection tasks for each parameter. In the first step, the estimates of (m,n,u,w') are obtained by finding a global maximum of $\Psi^I(a,b,c,d')$ over (a,b,c,d')

$$(\hat{m},\hat{n},\hat{u},\hat{w}') = \arg\max_{(a,b,c,d')} \Psi^I(a,b,c,d') \tag{18}$$

A close look at (18) indicates that the search space of d' can be reduced by half since $d' \in \{3,4,\cdots,65\}$, which allows a decrease in the computational burden of the proposed NSSS detection scheme. In this step, the estimate of the RFN can be obtained from combining $\hat{m}$ and $\hat{u}$, and it is tentatively decided that the NSSS with ZC root index $\hat{w}'$ or $131-\hat{w}'$ was transmitted from the eNodeB. Based on the estimates $(\hat{m},\hat{n},\hat{u},\hat{w}')$, the NB-IoT UE attempts to determine which NSSS was actually transmitted during the second step. To end this, the NB-IoT UE performs the task given by

$$\hat{w}'' = \arg\max_{w''} \Omega^I(\hat{m},\hat{n},\hat{u},w'') \tag{19}$$

where $w'' \in \{\hat{w}', 131-\hat{w}'\}$ is the possible candidate for w that is tentatively selected from the first step. Due to only two hypothesized numbers of w, (19) is equivalently formulated by

$$\Omega^I(\hat{m},\hat{n},\hat{u},\hat{w}') \underset{131-\hat{w}'}{\overset{\hat{w}'}{\gtrless}} \Omega^I(\hat{m},\hat{n},\hat{u},131-\hat{w}') \tag{20}$$

Using (12), the decision statistic can be rewritten as

$$\Omega^I(\hat{m},\hat{n},\hat{u},\hat{w}') - \Omega^I(\hat{m},\hat{n},\hat{u},131-\hat{w}') = 2\sum_{k\in\mathcal{S}}\sum_{l=\hat{m}N_f+3}^{\hat{m}N_f+13}\tilde{Y}_{l,k}^{Q}E_{l,k}^{Q}(\hat{n},\hat{u},\hat{w}') \tag{21}$$

which is based on the second term of the RHS in (12). Then, the decision rule of (20) is equivalently represented as

$$\sum_{k\in\mathcal{S}}\sum_{l=\hat{m}N_f+3}^{\hat{m}N_f+13}\tilde{Y}_{l,k}^{Q}E_{l,k}^{Q}(\hat{n},\hat{u},\hat{w}') \underset{131-\hat{w}'}{\overset{\hat{w}'}{\gtrless}} 0 \tag{22}$$

which does not involve additional complexity since it has been already computed in (14) and it can be performed only by checking the sign of $\sum_{k\in\mathcal{S}}\sum_{l=\hat{m}N_f+3}^{\hat{m}N_f+13}\tilde{Y}_{l,k}^{Q}E_{l,k}^{Q}(\hat{n},\hat{u},\hat{w}')$. Based on this observation, w is estimated by $\hat{w}''=\hat{w}'$ or $131-\hat{w}'$ according to the decision rule (22). As a result, the estimate of v can be given by $\hat{v}=126\hat{n}+\hat{w}''-3$ after obtaining $\hat{n}$ and $\hat{w}''$ from (18) and (22), respectively.

4.2. Detection Performance

We derive the PED as a performance measure assuming a flat-fading channel. Under hypothesis H_1, conditioned on $\alpha=|H_{l,k}|^2$, it can be effortlessly seen that the decision variable $\sum_{k\in\mathcal{S}}\sum_{l=aN_f+3}^{aN_f+13}\tilde{Y}_{l,k}^{I/Q}E_{l,k}^{I/Q}(b,c,d') \sim \mathcal{G}(\mu_{f1},\sigma_{f1}^2)$ with $\mu_{f1}=\alpha N_s E_X/2$ and $\sigma_{f1}^2=\alpha N_s E_X\sigma_Z^2/4$. Thus, it is observed that $|\sum_{k\in\mathcal{S}}\sum_{l=aN_f+3}^{aN_f+13}\tilde{Y}_{l,k}^{Q}E_{l,k}^{Q}(b,c,d')|$ has a folded normal probability density function (PDF) denoted as

$$f(x|H_1)=\sqrt{\frac{2}{\pi\sigma_{f2}^2}}e^{-\frac{x^2+\mu_{f2}^2}{2\sigma_{f2}^2}}\cosh\left(\frac{x\mu_{f2}}{\sigma_{f2}^2}\right),\ x\geq 0 \tag{23}$$

where $\mu_{f2}=\sigma_{f1}\sqrt{2/\pi}e^{-\mu_{f1}^2/2\sigma_{f1}^2}+\mu_{f1}[1-2Q(\mu_{f1}/\sigma_{f1})]$ and $\sigma_{f2}^2=\mu_{f1}^2+\sigma_{f1}^2-\mu_{f2}^2$. For $N_s\gg 1$, we can safely say that $\Psi^I(a,b,c,d')\sim\mathcal{G}(\mu_{h1},\sigma_{h1}^2)$ with $\mu_{h1}=\mu_{f1}+\mu_{f2}$ and $\sigma_{h1}^2=\sigma_{f1}^2+\sigma_{f2}^2=\mu_{f1}^2+2\sigma_{f1}^2-\mu_{f2}^2$. Denote the PDF of $\Psi^I(a,b,c,d')$ under hypothesis H_1 as $f(x|H_1)$. On the other hand, $\sum_{k\in\mathcal{S}}\sum_{l=aN_f+3}^{aN_f+13}\tilde{Y}_{l,k}^{I/Q}E_{l,k}^{I/Q}(b,c,d')\sim\mathcal{G}(0,\sigma_{h0}^2)$ with $\sigma_{h0}^2=\alpha^2N_sE_X^2/4+\alpha N_sE_X\sigma_Z^2/4$ in the case of hypothesis H_0. Accordingly, $\Psi^I(a,b,c,d')$ under hypothesis H_0 obeys a skew normal distribution with PDF and cumulative distribution function written, respectively, as [24]

$$f(x|H_0)=\frac{1}{\sqrt{\pi\sigma_{h0}^2}}e^{-\frac{x^2}{4\sigma_{h0}^2}}\left[1-Q\left(\frac{x}{\sqrt{2}\sigma_{h0}}\right)\right] \tag{24}$$

and

$$F(x|H_0)=\left[1-Q\left(\frac{x}{\sqrt{2}\sigma_{h0}}+\frac{\mu_{h1}}{\sqrt{2}\sigma_{h0}}\right)\right]^2 \tag{25}$$

In the first stage, we write the PED of (18) as $P_{f1}=\text{Prob}\{(\hat{m},\hat{n},\hat{u},\hat{w}')\neq(m,n,u,w')\}$. Using a folded normal and a skew normal distributions under hypothesis H_1 and hypothesis H_0, respectively, $P_{f1}(\alpha)$ conditioned on α is obtained as

$$P_{f1}(\alpha)\approx 1-\sum_{z=0}^{4030}(-\beta_0)^z\binom{4030}{z}\frac{1}{\sqrt{1+z\beta_2\sigma_{h1}^2/\sigma_{h0}^2}}e^{-\frac{\mu_{h1}^2}{4\sigma_{h0}^2}}e^{\frac{1}{4}\left(\frac{\mu_{h1}}{\sigma_{h0}}-z\beta_1\frac{\sigma_{h1}}{\sigma_{h0}}\right)^2/\sqrt{1+z\beta_2\sigma_{h1}^2/\sigma_{h0}^2}} \tag{26}$$

with

$$\frac{\sigma_{h1}^2}{\sigma_{h0}^2} = \frac{N_s\gamma+2}{\gamma+1} - \frac{1}{\gamma+1}\left(\sqrt{\frac{2}{\pi}}e^{-\frac{N_s\gamma}{2}} + \sqrt{N_s\gamma}\left[1-2Q\left(\sqrt{N_s\gamma}\right)\right]\right)^2 \tag{27}$$

and

$$\frac{\mu_{h1}^2}{\sigma_{h0}^2} = \frac{1}{\gamma+1}\left(\sqrt{\frac{2}{\pi}}e^{-\frac{N_s\gamma}{2}} + \sqrt{N_s\gamma}\left[1-Q\left(\sqrt{N_s\gamma}\right)\right]\right)^2 \tag{28}$$

where $\gamma = \alpha^2 E_X/\sigma_Z^2$ denotes the SNR. The detail of the derivation of (26) is provided in Appendix A.

In the second step, denote the PED of (19) by $P_{f2} = \text{Prob}\{\hat{w}'' \neq w\}$. Similarly, $\Omega^I(a,b,c,d) \sim \mathcal{G}(\mu_{h1}, \sigma_{h1}^2)$ under hypothesis H_1, while $\Omega^I(a,b,c,d) \sim \mathcal{G}(0, 2\sigma_{h0}^2)$ under hypothesis H_0. Thus, $P_{f2}(\alpha)$ is given in an identical form to (A2) with 4030 replaced by 1, which has a closed-form solution

$$P_{f2}(\alpha) = Q\left(\frac{\mu_{h1}}{\sqrt{2\sigma_{h0}^2+\sigma_{h1}^2}}\right) \tag{29}$$

To obtain unconditional probability expression, one averages over the distribution of α expressed as $f_\alpha(x) = (1/\sigma_H^2)e^{-x/\sigma_H^2}$, leading to $P_{fi} = \int_0^\infty P_{fi}(x)f_\alpha(x)dx$ $(i = 1, 2)$. As a consequence, the proposed method erroneously detects the NSSS with a probability of $P_f = P_{f1} \times P_{f2}$.

5. Simulation Results and Discussions

This section provides analysis and simulation results to demonstrate the performance of the coherent NSSS detection algorithm in the NB-IoT system. Matlab software was used as a simulation platform to verify the proposed algorithm.

5.1. Simulation Environment

Let us consider the NB-IoT system with a system bandwidth of 180 kHz and 15 kHz minimum subcarrier spacing at the 900 MHz band. In the following, the DFT size is equal to $N = 128$, and the CP size is equal to $N_g = 10$. The 128-point DFT includes 12 NSSS subcarriers and 58 guard-band subcarriers. The sampling time period is $T_s = 0.52$ µs, and the length of the NSSS sequence is $N_s = 132$. Table 2 shows the system parameters used in the simulation. Based on the simulation parameters, the processing frequency is 1.92 MHz, and a 128-point DFT transforms the time-domain signals into frequency-domain signals [25]. For simulation, we consider two representative channels such as Pedestrian and Vehicular models to verify the capability of the presented NSSS detectors [26]. Since most of the NB-IoT terminals move slowly, we assume that a maximum Doppler frequency is equal to 1 Hz for the Pedestrian channel model [14,25]. On the other hand, the Doppler frequency of 55 Hz is considered in the Vehicular channel, which corresponds to a maximum mobile speed of 60 km/h [27]. For multipath channels, the magnitude of each tap is Rayleigh distributed and the Doppler power spectrum for each tap is characterized by a classical Jakes model. Table 3 shows the channel profile used for simulation. As for residual CFO and STO, we set $\varepsilon = 0.02$, and ϑ is uniformly generated from $[0, N_g/2]$. Simulations have been conducted over 10^6 radio frames for independent channel realizations.

Table 2. Simulation parameters.

Parameters	Values
Carrier frequency	900 MHz
Transmission bandwidth	180 kHz
DFT size	$N = 128$
Number of CP samples	$N_g = 10$
Number of samples in one OFDM symbol	$N_t = 138$
Sampling time period	$T_s = 0.52$ µs
Subcarrier spacing	$\Delta_f = 15$ kHz
Length of NSSS sequence	$N_s = 132$

Table 3. Channel models.

Channel Model	Maximum Delay Spread
Pedestrian A (PedA)	0.41 µs
Pedestrian B (PedB)	3.7 µs
Vehicular A (VehA)	2.15 µs
Vehicular B (VehB)	19.8 µs

5.2. Benchmark Method

For comparison, we introduce three conventional NSSS detectors. The first one is a low-complexity PCID and RFN detection (LPRD) scheme developed in [14], which is based on the non-coherent objective function

$$\Lambda_1(a,b,c,d) = \sum_{k\in\mathcal{S}} \sum_{l=aN_f+3}^{aN_f+13} Y_{l,k} E^*_{l,k}(b,c,d) \tag{30}$$

In the LRPD method, (n,u,w,m) are detected by maximizing $|\Lambda_1(a,b,c,d)|$ over hypothesized numbers (a,b,c,d), and this method has been proposed assuming a frequency-flat fading channel. Under hypothesis H_1, $|\Lambda_1(a,b,c,d)|$ follows a Rician distribution with mean $\mu = 2\mu_{f1}$ and variance $\sigma_1^2 = 4\sigma_{f1}^2$, while $|\Lambda_1(a,b,c,d)|$ follows a Rayleigh distribution with variance $\sigma_0^2 = 4\sigma_{h0}^2$ in the case of hypothesis H_0. Identically, the PED of the LPRD method can be obtained as

$$P_f(\alpha) = 1 - \int_0^\infty 2x(\gamma+1)e^{-(\gamma+1)x^2 - N_s\gamma} I_0\left(2x\sqrt{N_s\gamma(\gamma+1)}\right)\left[1-e^{-x^2}\right]^{4031} dx \tag{31}$$

The second benchmark benchmark is a sequential PCID and RFN detection (SPRD) scheme, which decouples the detection of $B_{l,k}(n)$ and $C_{l,k}(u)D_{l,k}(w)$ [17]. Based on the observation that $n = 2n' + n'' \in \{0,1,2,3\}$ for $n' \in \{0,1\}$ and $n'' \in \{0,1\}$, the PCID and RFN are detected by searching for maximum of two objective functions, respectively

$$\Lambda_2(a,b',c,d) = \sum_{k\in\mathcal{S}} \sum_{l=aN_f+3}^{aN_f+13} Y_{l,k} \sum_{b''=0}^{1} B^*_{l,k}(2b'+b'')C^*_{l,k}(c)D^*_{l,k}(d) \tag{32}$$

and

$$\Lambda_3(b'') = \sum_{k\in\mathcal{S}} \sum_{l=\hat{m}N_f+3}^{\hat{m}N_f+13} Y_{l,k} B^*_{l,k}(2\hat{n}'+b'')C^*_{l,k}(\hat{u})D^*_{l,k}(\hat{w}) \tag{33}$$

where $b' \in \{0,1\}$ and $b'' \in \{0,1\}$ denote the possible combinations of n' and n'', respectively [17]. Consequently, $(\hat{m},\hat{u},\hat{w})$ are estimated by maximizing $|\Lambda_2(a,b',c,d)|$ subject to (a,b',c,d), while $\hat{n}'$ and $\hat{n}''$ are obtained by finding the maximum argument of $|\Lambda_2(a,b',c,d)|$ and $|\Lambda_3(b'')|$, respectively, leading to $\hat{n} = 2\hat{n}' + \hat{n}''$. The last benchmark is

a DFT-based PCID and RFN detection (DPRD) scheme proposed in [20]. Denoting the channel coefficient as $H_{l,k} = |H_{l,k}|e^{j\theta_k}$, the estimate of θ_k is obtained by

$$\hat{\theta}_k(a,b,c,d) = \angle\left\{\sum_{l=aN_f+3}^{aN_f+13} Y_{l,k}E^*_{l,k}(b,c,d)\right\},\ k \in \mathcal{S} \tag{34}$$

Based on the estimated channel (34) and the objective function (8) with $\tilde{Y}_{l,k}(a,b,c,d)$ replaced by $Y_{l,k}e^{-j\hat{\theta}_k(a,b,c,d)}$, the DPRD method obtains the estimates of the PCID and RFN by maximizing $\Omega^I(a,b,c,d)$ over (a,b,c,d). Assuming a perfectly known channel, it follows that $\Omega^I(a,b,c,d) \sim \mathcal{G}(\mu, \sigma_1^2/2)$ under hypothesis H_1 and $\Omega^I(a,b,c,d) \sim \mathcal{G}(0, \sigma_0^2/2)$ under hypothesis H_0. In this case, the PED of the DPRD method can be expressed as

$$P_f(\alpha) = 1 - \int_{-\infty}^{\infty} \frac{1}{\sqrt{2\pi}} e^{-\frac{x^2}{2}} \left[1 - Q\left(\frac{x + \sqrt{N_s\gamma}}{\sqrt{\gamma+1}}\right)\right]^{4031} dx \tag{35}$$

5.3. Complexity Evaluation

In order to have a fair comparison with benchmark systems, it is assumed that $B_{l,k}(b)C_{l,k}(c)$ produces 16 combined complementary sequences, which only have values of ± 1 or $\pm j$ [14], and thus, any extra complexity is not required because these sequences are processed only by sign inversions. Moreover, suppose one complex multiplication (CM) is equivalent to six real multiplications (RMs) [28].

We first compute the arithmetic complexity of the LPRD method. Let us denote N_v as the number of average estimates. Since $D_{l,k}(c)$ is conjugate symmetric with respect to the origin, $|\Lambda_1(a,b,c,d)|$ requires $N_s/2$ CMs and the number of hypotheses requiring CM operation is 252. Applying N_v-times average estimation, the LPRD method obtains the PCID and RFN with $16632N_v$ CMs. Next, we compute the number of CMs used in the SPRD method. Since the SPRD method does not involve any CM for the NSSS subcarriers that meet the formulation $\sum_{b''=0}^{1} B_{l,k}(2b' + b'') = 0$, $|\Lambda_2(a,b',c,d)|$ and $|\Lambda_3(b'')|$ are processed with $N_s/4$ and $N_s/2$ CMs for each hypothesis, respectively. Applying all hypotheses and N_v-times average estimation, $8382N_v$ CMs are required to sequentially complete the SPRD. As mentioned earlier, the DPRD method is based on both the observations (8) and (34). For each hypothesis, (34) requires N_s CMs for computing the quantity $\sum_{l=aN_f+3}^{aN_f+13} Y_{l,k}E^*_{l,k}(b,c,d)$ and $N_s/11$ CMs for implementing the argument operation $\angle\{\cdot\}$, while $2N_s/11$ RMs are used for (8) since some quantities have been already evaluated in (34). The number of hypotheses requiring CM operation is 252 for computing the quantity $\sum_{l=aN_f+3}^{aN_f+13} Y_{l,k}E^*_{l,k}(b,c,d)$, 4032 for implementing $\angle\{\cdot\}$, and 4032 for (8). This leads to a total complexity of $97776N_v$ CMs, which corresponds to the complexity of the DRPD method that can combat frequency-selective fading. As reported in [20], the DPRD approach can be processed utilizing DFT operations with almost equal complexity as the LPRD approach if the channel is considered to be frequency-flat.

Finally, we assess the computational load of the proposed method. For each hypothesis, (7) and (14) require N_s CMs and $2N_s/11$ RMs, respectively. Similar to the DPRD, (7) has to be hypothesized for 252 combinations, while (14) is hypothesized for only 2016 possible candidates. Considering all hypotheses associated with (18), $252N_s$ CMs and $4032N_s/11$ RMs are required in the first stage. Recalling from (22) that (19) can be implemented without any CM in the second stage, the overall number of CMs is equal to $41328N_v$.

5.4. Performance Evaluation

In Figure 1, the PED of the benchmark and proposed NSSS detection schemes is plotted as a function of SNR in the AWGN and flat-fading channel models. To focus on evaluating the analysis derived in Section 4.2, it is assumed that $\varepsilon = \vartheta = 0$ and the channel is perfectly estimated. The first observation from this figure is that analytical results

completely agree with simulation results for both AWGN and flat-fading channels. As expected, an average over multiple NSSS observations can be used to reduce noise impact on the final estimate. It can be clearly seen that the DPRD method outperforms the LPRD method regardless of the channel model and N_v, while the PED of the proposed detector is slightly better than that of the DPRD method. In the case of the coherent approaches such as the DPRD and proposed methods, it is observed that the performance gain due to the average estimate is more significant compared to the LPRD method. However, imperfect channel estimation degrades the detection performance of the coherent methods, which will be discussed below.

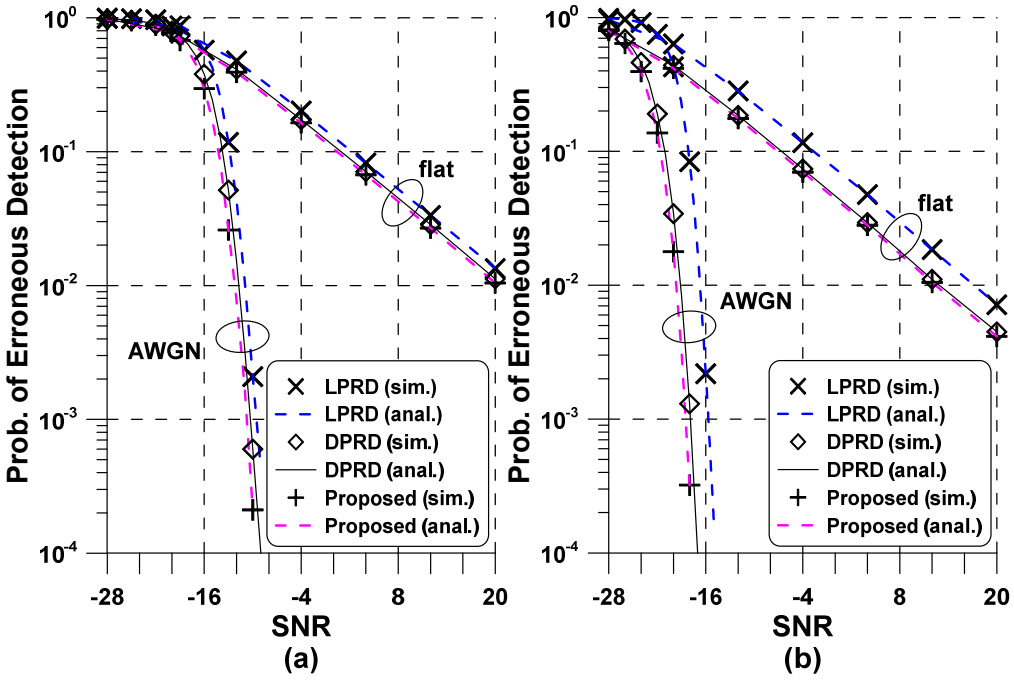

Figure 1. PED of the NSSS detectors in the AWGN and flat-fading channels: (**a**) $N_v = 1$ (**b**) $N_v = 11$.

In Figure 2, the PED of the benchmark and proposed NSSS detection algorithms is plotted versus SNR in the PedA and PedB channel models. For the average estimate, we set $N_v = 11$ in the following. From the observations in Figure 2, the channel estimation error mainly degrades the detection performance for the coherent detection approaches if ignoring the AWGN. If the channel is perfectly known, the performance of coherent detection methods is better than that of non-coherent LPRD and SPRD methods regardless of the channel models. However, using the estimated channel degrades the detection ability of the coherent detection schemes due to the channel estimation error in the PedA channel. Therefore, accurate channel estimation is essential for the DPRD and proposed methods to robustly detect the NSSS. Both coherent approaches differ in the method of estimating the channel, as described in (7) and (34), which leads to a performance difference. As predicted, the PED of non-coherent methods is not affected by the knowledge of the channel. In the PedB channel, an irreducible error floor can be observed for non-coherent approaches as the SNR increases, which is eventually the dominant performance degrading factor for the LPRD and SPRD methods. This phenomenon is mainly explained by the fact that the LPRD and SPRD schemes do not combat the frequency-selective fading because they are originally developed assuming flat-fading conditions. Since a maximum delay spread of 0.41 μs in the PedA channel is less than the sampling time interval of 0.52 μs, it can be considered to be a flat-fading channel.

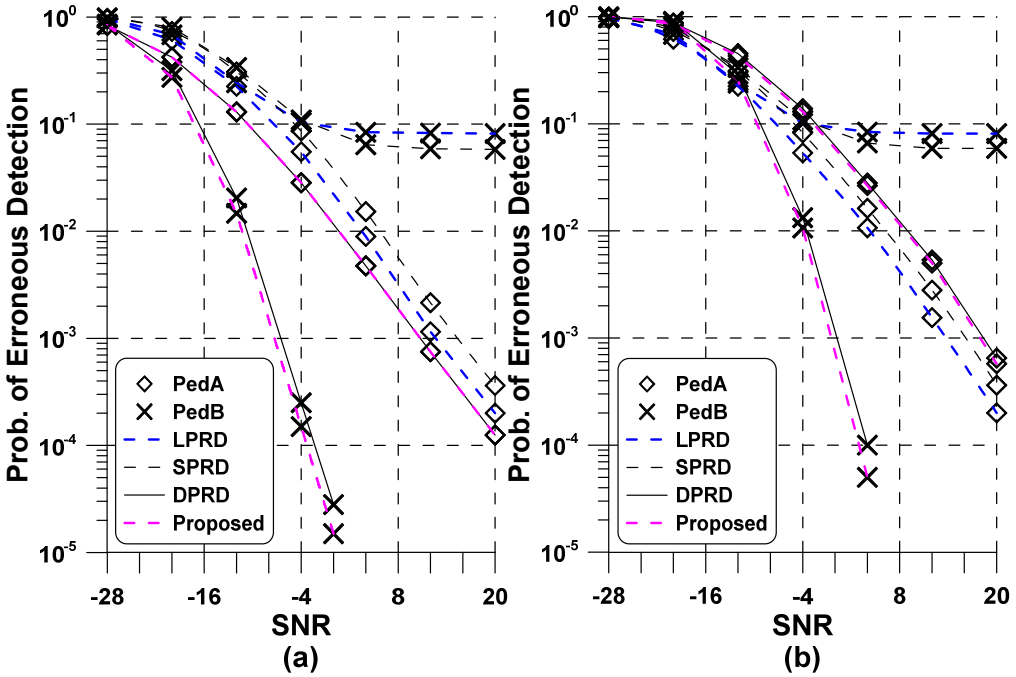

Figure 2. Performance comparison of the benchmark and proposed methods in the pedestrian channel models: (**a**) perfect channel (**b**) estimated channel.

Figure 3 displays the PED of the benchmark and proposed NSSS detection methods versus SNR in the VehA and VehB channel models. We adopt the same simulation setting as in Figure 2, except for a sufficiently larger delay spread with respect to the pedestrian channel. It is seen from Figure 3 that the proposed method outperforms the LPRD method with the increase in SNR, while it shows similar behavior to the DPRD method. When compared to the PED in the PedA channel, the coherent detection methods have improved performance regardless of the channel models. On the contrary, non-coherent detection methods exhibit irreducible error floor due to increased frequency selectivity of the channel. These observations show the robustness of the proposed detection method under various channel fading conditions. Such a gain is a consequence of the multipath diversity that becomes more outstanding in the vehicular channel due to a larger delay spread in comparison with the pedestrian channel. Conversely, the effect of the multipath diversity is diminished in the case of the VehB channel, even though the VehB channel experiences more frequency-selective fading than the VehA channel. This is basically due to the fact that the maximum delay spread of 19.8 μs in the VehB channel exceeds the CP duration of 5.2 μs, thus incurring both the inter-symbol interference and ICI.

Figure 4 shows the PED performance of the NSSS detectors when SNR $= -5$ dB and SNR $= 0$ dB. To quantify the performance gap between the detection methods, denote the number of averaged radio frames required to achieve a target error probability of 10% as N_f. In the case of the VehA channel, $N_f = 5$ is for the LPRD, DPRD, and proposed methods when NB-IoT UEs are in a poor coverage condition of SNR $= -5$ dB. However, the performance gap between the LPRD and proposed approaches becomes larger as N_f increases, with the latter showing a better performance when compared to the former. In light of the same value of N_f, the complexity of the proposed scheme is reduced by 57.7% and increases 2.5 times compared to that of the DPRD and LPRD methods, respectively. Generally, power consumption is proportional to the number of floating point operations (flops) used to design the NSSS detectors [29]. Therefore, it can be expected that a reduced number of flops of the proposed NSSS detector enhances the power consumption efficiency if other system parameters determining power consumption are the same. As discussed earlier, the non-coherent detection method outperforms the coherent detection method in the PedA channel so that $N_f = 5$ for the LPRD, $N_f = 10$ for the SPRD, and $N_f = 15$ for the

proposed method. More interestingly, the average effect is marginal in the PedA channel regardless of detection approaches, which is caused by the flat fading condition, while the average effect becomes larger in the frequency-selective channel, similar to the VehA channel. By applying the proposed detection strategy to the NB-IoT system, the arithmetic complexity of the initial synchronization receiver can be decreased, and it substantially reduces power consumption, ultimately extending the battery life of NB-IoT UEs.

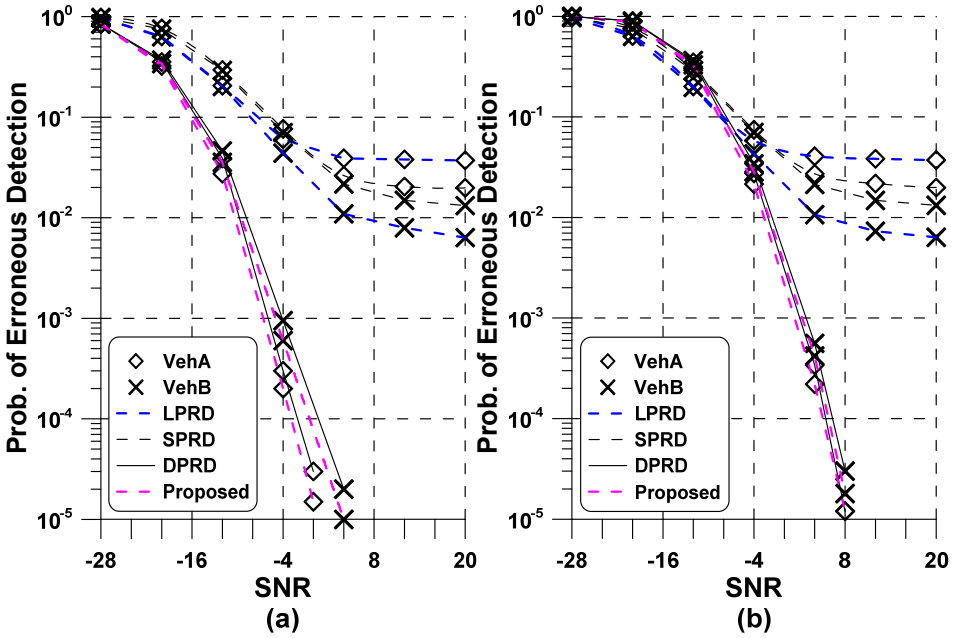

Figure 3. Performance comparison of the benchmark and proposed methods versus SNR in the vehicular channel models: (**a**) perfect channel (**b**) estimated channel.

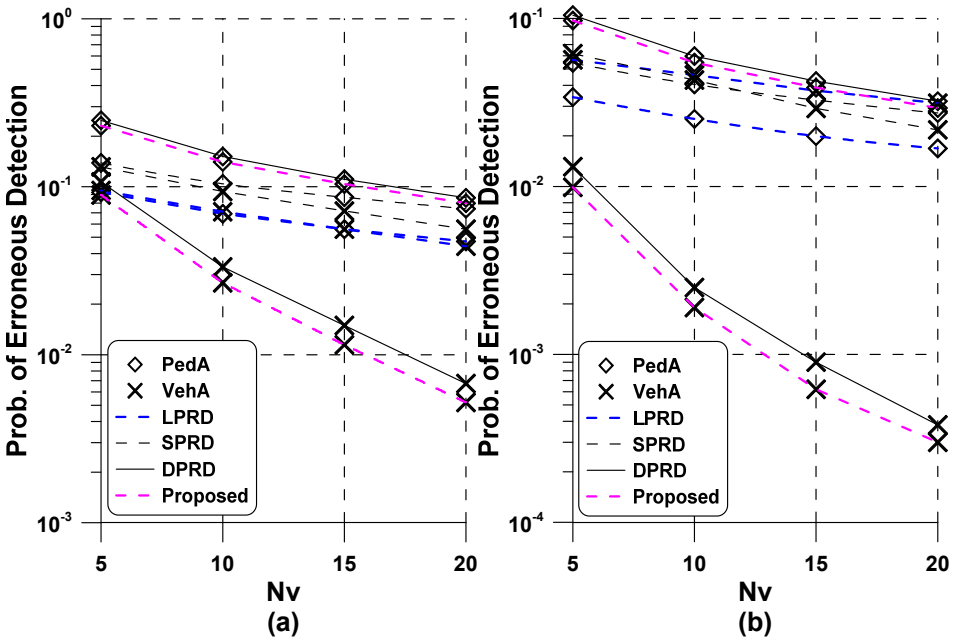

Figure 4. Performance comparison of the benchmark and proposed methods versus N_v: (**a**) SNR $= -5$ dB (**b**) SNR $= 0$ dB.

6. Conclusions

In this study, we have proposed a low-complexity coherent NSSS detection scheme in the cellular NB-IoT system. To alleviate the computational load associated with the

conventional coherent detection method, the search space of NSSS hypothesis testing is reduced by decoupling the detection of the PCID and RFN. Simulation results were provided not only to show the correctness of numerical analysis but also to validate the improved performance of the proposed coherent NSSS detection scheme. It has been shown that the theoretical and simulation results are in excellent agreement. Moreover, we have compared the proposed NSSS detection method with the conventional NSSS detection methods in terms of the computational complexity and detection performance. From simulation results, it has been verified that the proposed solution not only attains nearly the same performance as the existing NSSS detection method but also significantly reduces the computational complexity. To achieve a target error rate of 10% in the Pedestrian channel model, it has been shown that the number of CMs of the proposed method is reduced by more than 50% in a poor coverage area compared to the DPRD method. Furthermore, it has been summarized that the presented NSSS detection methods use fewer radio frames to attain a target detection rate and the effect of the average estimate becomes more pronounced in the vehicular channel model.

Author Contributions: Conceptualization, Y.-H.Y. and Y.-A.J.; methodology, Y.-H.Y. and Y.-A.J.; software, Y.-A.J.; writing—original draft preparation, Y.-H.Y. and Y.-A.J.; writing—review and editing, Y.-H.Y., Y.-A.J., S.-H.L. and I.H.; visualization, Y.-H.Y., Y.-A.J. and I.H.; supervision, Y.-H.Y. All authors have read and agreed to the published version of the manuscript.

Funding: This work was in part supported by the Institute of Information and communications Technology Planning and Evaluation (IITP) grant funded by the Korean government (MSIT) (No. 2022-0-00868, Development of High-Resolution Vector Network Analyzer HW Platform Supporting Sub-THz Frequency Band) and in part by the Basic Science Research Program through the National Research Foundation of Korea (NRF) funded by the Ministry of Education (2021R1F1A1057577).

Institutional Review Board Statement: Not applicable.

Informed Consent Statement: Not applicable.

Data Availability Statement: Not applicable.

Conflicts of Interest: The authors declare no conflict of interest.

Appendix A. Derivation of PED

The conditional PED on α is given by

$$P_{f1}(\alpha) = 1 - \int_{-\infty}^{\infty} f(x|H_1)[F(x|H_0)]^{2015} dx \tag{A1}$$

After substituting (23) and (25) into (A1) and performing some manipulations, one readily finds that

$$P_{f1}(\alpha) = 1 - \int_{-\infty}^{\infty} \frac{1}{\sqrt{2\pi}} e^{-\frac{x^2}{2}} \left[1 - Q\left(\frac{\sigma_{h1}}{\sqrt{2}\sigma_{h0}} x + \frac{\mu_{h1}}{\sqrt{2}\sigma_{h0}}\right)\right]^{4030} dx \tag{A2}$$

To obtain a closed-form expression of (A2), we adopt an exponential approximation of $Q(x)$ as follows

$$Q\left(\frac{\sigma_{h1}}{\sqrt{2}\sigma_{h0}} x + \frac{\mu_{h1}}{\sqrt{2}\sigma_{h0}}\right) \approx \beta_0 e^{-\beta_1\left(\frac{\sigma_{h1}}{\sqrt{2}\sigma_{h0}} x + \frac{\mu_{h1}}{\sqrt{2}\sigma_{h0}}\right)} e^{-\beta_2\left(\frac{\sigma_{h1}}{\sqrt{2}\sigma_{h0}} x + \frac{\mu_{h1}}{\sqrt{2}\sigma_{h0}}\right)^2} \tag{A3}$$

where $\beta_0 = 0.49$, $\beta_1 = 8/13$, and $\beta_2 = 1/2$ are the fitting parameters [30]. Inserting (A3) into (A2) and applying binomial expansion, $P_{f1}(\alpha)$ can be approximated as

$$P_{f1}(\alpha) \approx 1 - \sum_{z=0}^{4030} (-\beta_0)^z \binom{4030}{z} U(z) \tag{A4}$$

where

$$U(z) = \frac{1}{\sqrt{2\pi}} \int_{-\infty}^{\infty} e^{-\frac{x^2}{2}} e^{-z\beta_1 \left(\frac{\sigma_{h1}}{\sqrt{2}\sigma_{h0}} x + \frac{\mu_{h1}}{\sqrt{2}\sigma_{h0}} \right)} e^{-z\beta_2 \left(\frac{\sigma_{h1}}{\sqrt{2}\sigma_{h0}} x + \frac{\mu_{h1}}{\sqrt{2}\sigma_{h0}} \right)^2} dx \tag{A5}$$

We can effortlessly find from [31] that

$$U(z) = \frac{1}{\sqrt{1 + z\beta_2 \sigma_{h1}^2 / \sigma_{h0}^2}} e^{-\frac{\mu_{h1}^2}{4\sigma_{h0}^2}} e^{\frac{1}{4} \left(\frac{\mu_{h1}}{\sigma_{h0}} - z\beta_1 \frac{\sigma_{h1}}{\sigma_{h0}} \right)^2 / \sqrt{1 + z\beta_2 \sigma_{h1}^2 / \sigma_{h0}^2}} \tag{A6}$$

From (A4)∼(A6), we obtain the final PED expression of (26).

References

1. 3GPP, TR 45.820, V13.1.0, Cellular System Support for Ultra-Low Complexity and Low Throughput Internet of Things (CIoT). 2015. Available online: https://portal.3gpp.org/desktopmodules/Specifications/SpecificationDetails.aspx?specificationId=2719 (accessed on 18 August 2022).
2. Dangana, M.; Ansari, S.; Abbasi, Q.H.; Hussain, S.; Imran, M.A. Suitability of NB-IoT for indoor industrial environment: A survey and insights. *Sensors* **2021**, *21*, 5284. [CrossRef] [PubMed]
3. Haider, S.K.; Nauman, A.; Jamshed, M.A.; Jiang, A.; Batool, S.; Kim, S.W. Internet of drones: Routing algorithms, techniques and challenges. *Mathematics* **2022**, *10*, 1488. [CrossRef]
4. Chen, X.; Zhao, T.; Sun, Q.; Hu, Q.; Xu, M. Cell-free massive MIMO with energy-efficient downlink operation in industrial IoT. *Mathematics* **2022**, *10*, 1687. [CrossRef]
5. 3GPP, TR 36.888, Study on Provision of Low-Cost Machine-Type Communications (MTC) User Equipments (UEs) Based on LTE. 2013. Available online: https://portal.3gpp.org/desktopmodules/Specifications/SpecificationDetails.aspx?specificationId=2578 (accessed on 18 August 2022).
6. Almuhaya, M.A.M.; Jabbar, W.A.; Sulaiman, N.; Abdulmalek, S. A Survey on LoRaWAN technology: Recent trends, opportunities, simulation tools and future directions. *Electronics* **2022**, *11*, 164. [CrossRef]
7. 3GPP, 3GPP TS 36.211, Physical Channels and Modulation (Release 14); Tech. Rep. 2017. Available online: https://portal.3gpp.org/desktopmodules/Specifications/SpecificationDetails.aspx?specificationId=2425 (accessed on 18 August 2022).
8. Lujan, E.; Zuloaga Mellino, J.A.; Otero, A.D.; Vega, L.R.; Galarza, C.G.; Mocskos, E.E. Extreme coverage in 5G narrowband IoT: A LUT-based strategy to optimize shared channels. *IEEE Internet Things J.* **2020**, *7*, 2129–2136. [CrossRef]
9. Aghazadeh Ayoubi, R.; Spagnolini, U. Performance of dense wireless networks in 5G and beyond using stochastic geometry. *Mathematics* **2022**, *10*, 1156. [CrossRef]
10. Chang, K.; Lee, S. Robust OFDM-based synchronization against very high fractional CFO and time-varying fading. *IEEE Syst. J.* **2020**, *14*, 4047–4058. [CrossRef]
11. Yang, W.; Hua, M.; Zhang, J.; Xia, T.; Zou, J.; Jiang, C.; Wang, M. Enhanced system acquisition for NB-IoT. *IEEE Access* **2017**, *5*, 13179–13191. [CrossRef]
12. Intel Corporation. *Synchronization and Cell Search in NB-IoT: Performance Evaluation*; 3GPP TSG RAN WG1, Tech. Rep. R1-161898; Intel Corporation: Santa Clara, CA, USA, 2016.
13. Ali, A.; Hamouda, W. On the cell search and initial synchronization for NB-IoT LTE systems. *IEEE Commun. Lett.* **2017**, *21*, 1843–1846. [CrossRef]
14. Li, Y.; Chen, S.; Ye, W.; Lin, F. A joint low-power cell search and frequency tracking scheme in NB-IoT systems for green Internet of Things. *Sensors* **2018**, *18*, 3274. [CrossRef]
15. You, Y.H. Reduced complexity detection of narrowband secondary synchronization signal for NB-IoT communication systems. *Symmetry* **2020**, *8*, 1342. [CrossRef]
16. Savaux, V.; Kanj, M. Low-complexity sub-optimal cell ID estimation in NB-IoT system. *IET Commun.* **2020**, *14*, 3699–3706. [CrossRef]
17. You, Y.H.; Jung, Y.A.; Choi, S.C.; Hwang, I. Complexity effective sequential detection of synchronization signal for cellular narrowband IoT communication systems. *IEEE Internet Things J.* **2021**, *8*, 2900–2909. [CrossRef]
18. You, Y.H.; Jung, Y.A.; Lee, S.H.; Song, H.G.; Song, H.K. Balanced-offset joint acquisition of physical cell identity and radio frame number for NB-IoT communication systems. *IEEE Internet Things J.* **2022**, *11*, 8669–8680. [CrossRef]
19. Jung, Y.A.; Shin, D.; You, Y.H. A computationally efficient joint cell search and frequency synchronization scheme for LTE machine-type communications. *Symmetry* **2019**, *11*, 1394. [CrossRef]
20. Savaux, V. DFT-based low-complexity optimal cell ID estimation in NB-IoT. *EURASIP J. Adv. Signal Process.* **2020**, *2020*, 14. [CrossRef]
21. Rotem, A.; Dabora, R. A novel low-complexity estimation of sampling and carrier frequency offsets in OFDM communications. *IEEE Access* **2020**, *8*, 194978–194991. [CrossRef]

22. You, Y.H.; Lee, S.; Lee, K. Effective time, frequency, and sidelink synchronization for cellular device-to-device communications. *IEEE Syst. J.* **2021**, *15*, 2938–2947. [CrossRef]
23. Popovic, B.M. Generalized chirp-like polyphase sequences with optimum correlation properties. *IEEE Trans. Inf. Theory* **1992**, *30*, 769–777. [CrossRef]
24. Arellano-Vallea, R.B.; Genton, M.G. On fundamental skew distributions. *J. Multivariate Anal.* **2005**, *96*, 93–116. [CrossRef]
25. Jewel, M.K.H.; Zakariyya, R.S.; Lin, F. On channel estimation in LTE-based downlink narrowband Internet of Things systems. *Electronics* **2021**, *10*, 1246. [CrossRef]
26. International Telecommunication Union. *Guidelines for Evaluation of Radio Transmission Technologies for IMT-2000*; ITU-R M. 1225-97; International Telecommunication Union: Geneva, Switzerland, 1997.
27. Holfeld, B.; Wieruch, D.; Wirth, T.; Thiele, L.; Ashraf, S.A.; Huschke, J.; Aktas, I.; Ansari, J. Wireless communication for factory automation: An opportunity for LTE and 5G systems. *IEEE Commun. Mag.* **2016**, *54*, 36–43. [CrossRef]
28. Golub, G.H.; Loan, C.F.V. *Matrix Computations*, 4th ed.; The Johns Hopkins University Press: Baltimore, MD, USA, 2013.
29. Xiao, Z.; Zhao, J.; Liu, T.; Geng, L.; Zhang, F.; Tong, J. On the energy efficiency of massive MIMO systems with low-resolution ADCs and lattice reduction aided detectors. *Symmetry* **2020**, *12*, 406. [CrossRef]
30. Bao, V.N.; Tuyen, L.P.; Tue, H.H. A survey on approximations of one-dimensional Gaussian Q-function. *J. Electron. Commun.* **2015**, *5*, 1–14. [CrossRef]
31. Gradshteyn, I.S.; Ryzhik, I.M. *Table of Integrals, Series, and Products*; Academic Press: Cambridge, MA, USA, 2014.